Therapeutic implications of targeting cancer testis antigen MAGEA1 in cervical cancer

AYOUNG KIM[1,2*], JINA KIM[1,2*], WOORI KWAK[1,2*], KYUMIN MO[1,2], SOOHYUN CHOE[1,2], MINYEONG JEON[1,2], JISUN LEE[1], JUN-WON YUN[3] and HYUNHO YOON[1,2]

[1]Department of Medical and Biological Sciences, The Catholic University of Korea, Bucheon, Gyeonggi 14662, Republic of Korea; [2]Department of Biotechnology, The Catholic University of Korea, Bucheon, Gyeonggi 14662, Republic of Korea; [3]Laboratory of Veterinary Toxicology, College of Veterinary Medicine and Research Institute for Veterinary Science, Seoul National University, Seoul 08826, Republic of Korea

Received June 16, 2025; Accepted January 20, 2026

DOI: 10.3892/ijo.2026.5870

Abstract. MAGE family member A1 (MAGEA1), a cancer-testis antigen (CTA), is aberrantly expressed in several malignancies such as lung and liver cancers. However, its role in cervical cancer remains to be elucidated. The present study investigated the functional significance and therapeutic potential of MAGEA1 in cervical cancer using lentiviral short hairpin RNA-mediated knockdown, a series of functional assays, RNA sequencing (RNA-seq), and nude mouse xenograft models. It was found that MAGEA1 was upregulated in cervical cancer cells and its knockdown substantially suppressed cell proliferation, migration, invasion, and *in vivo* tumor growth. RNA-seq analysis further revealed that MAGEA1 silencing altered pathways related to apoptosis, DNA repair, and metabolism. Moreover, MAGEA1 knockdown enhanced chemosensitivity, indicating a potential role in mediating drug resistance. Collectively, the findings identified MAGEA1 as a key oncogenic driver in cervical cancer and highlighted its promise as both a prognostic biomarker and a therapeutic target, offering novel avenues for personalized treatment strategies in cervical cancer.

Correspondence to: Professor Jun-Won Yun, Laboratory of Veterinary Toxicology, College of Veterinary Medicine and Research Institute for Veterinary Science, Seoul National University, 1 Gwanak-ro, Gwanak, Seoul 08826, Republic of Korea
E-mail: jwyun@snu.ac.kr

Professor Hyunho Yoon, Department of Medical and Biological Sciences, The Catholic University of Korea, 43 Jibong-ro, Wonmi, Bucheon, Gyeonggi 14662, Republic of Korea
E-mail: hyoon@catholic.ac.kr

*Contributed equally

Key words: cancer testis antigen, MAGE family member A1, oncogene, cervical cancer, biomarker

Introduction

Cervical cancer is one of the most common gynecological carcinomas in the world with 569,847 cases and 311,365 mortalities annually (1). It ranks the second most prevalent lethal tumors in developing countries and the tenth in developed countries; in 2020, ~600,000 women were diagnosed with invasive cervical cancer, mostly in advanced stages (2). The World Health Organization (WHO) announced cervical cancer as a public health problem in May 2018. Cervical cancer is classified into two histological subtypes including squamous cell carcinoma (SCC) and adenocarcinoma (ADC) accounting for 68 and 21%, respectively. These two subtypes have different features in accordance with etiology, screening effectiveness, and prognosis (3). Accumulated studies have suggested that ADC exhibits worse prognosis compared with SCC (4). The major risk factors related to cervical cancer involve persistent human papilloma virus (HPV) infection, smoking, presence of sexual transmitted disease, such as human immunodeficiency virus or chlamydia infection (5). Despite early screening and vaccination, it remains the second leading cause of mortality in women aged 20-39 (6). There are critical individual differences in the prognosis of patients because of tumor heterogeneity. Thus, it is essential to investigate molecular heterogeneity and establish a complete prognostic assessment system, improving the precision treatment for cervical cancer.

Cancer testis antigens (CTAs) are specifically expressed in but abnormally expressed in some types of cancer including melanoma, lung cancer, liver cancer even in female cancer such as ovarian cancer and breast cancer (7-11). CTAs are expressed through embryonic development but abnormally re-expressed during tumorigenesis. Studies suggest that overexpression of oncogenic CTAs improves cancer cell stemness, tumorigenicity, metastasis, and drug resistance (12-15). The oncogenic CTAs provoke the initiation and development of malignant tumors (16). Physiological expression of CTAs in normal tissues is mostly limited to testis, and few are detected in normal adult somatic cells and tissues such as placental tissue (17). Until now, more than 200 CTAs have been identified and ~100 gene families are extremely expressed in

malignant tumors. Due to unique expression patterns, these CTAs are considered as immunogenic tumor-associated antigens promising targets for cancer treatment (18).

The first discovered gene among CTAs was the Melanoma Antigen gene (MAGE) family and is highly conserved in all eukaryotes. The MAGE family can be categorized in accordance with the pattern of tissue expression: Type I MAGEs are categorized as CTAs, including MAGE-A, -B, and -C subfamilies, whose genes are specifically located on the X chromosome. Type II MAGEs include MAGE-D to -L are expressed around various tissues in human body (19,20). Among the MAGE family, the role of MAGE-A groups is mostly unknown, exerting different functions in terms of subcellular localizations. Nonetheless, MAGEA1 is known to be located in the cytosol of melanoma cells and has also been detected in both the cytoplasm and nucleus of spermatogonia (21). MAGEA1 belongs to a cluster of 12 MAGE-A genes in X chromosome q28 region (22). Previous studies showed that promoter methylation and histone acetylation improve the expression of MAGEA1 in human cancer cells including lung cancer, breast cancer and colorectal cancer (23,24). However, detail functions are mainly unrevealed. Thus, this study aims to investigate the role of MAGEA1 in cervical cancer and its potential as a therapeutic target and biomarker.

Materials and methods

Survival prognosis analysis. Kaplan-Meier survival analysis was performed using the KM Plotter online database (https://kmplot.com/analysis/) to evaluate the prognostic significance of MAGEA1 expression levels in cancer patients. This publicly available platform contains comprehensive survival data, including overall survival information for patients with ovarian, lung, gastric, colon cancers, and cervical squamous cell carcinomas. Kaplan-Meier plots were generated to assess the correlation between MAGEA1 expression levels and patient survival outcomes across these cancer types.

Cells and cell culture. HeLa (CCL-2) and Panc1 (CRL-1469) were purchased from American Type Culture Collection. SK-OV-3 (cat. no. 30077), T24 (cat. no. 30004), SiHa (cat. no. 30035) were purchased from Korean Cell Line Bank. The cells were cultured in Dulbecco's modified Eagle's medium (Biowest) with 10% fetal bovine serum (Gibco; Thermo Fisher Scientific, Inc.) and 1% antibiotic-antimycotic (Gibco; Thermo Fisher Scientific, Inc.) in a humidified atmosphere of 5% CO_2 at 37˚C.

Reverse transcription-quantitative (RT-q) PCR. The total RNA was extracted from $1x10^6$ cells with TRIzol® reagent (Invitrogen; Thermo Fisher Scientific, Inc.). The concentration and quality of the total RNA were measured by Nanodrop (NanoDrop Technologies; Thermo Fisher Scientific, Inc.). For cDNA synthesis, the reverse transcription was performed using reverse transcription system (Promega Corporation). Primers for each target gene were designed by extracting the coding sequence from the corresponding NCBI reference sequence and generating forward and reverse primers accordingly. The primer sequences used in this study were as follows: MAGEA1 forward: 5'-AGGTGGCTGATTTGGTTGGT-3', reverse: 5'-GACCAGCTGCAAGGACTCAG-3'; β-actin forward: 5'-GCACTCTTCCAGCCTTCCTT-3', reverse: 5'-GTTGGCGTACAGGTCTTT GC-3'. The mRNA level of MAGEA1 was determined by qPCR according to triplicate with SYBR green mix (Bio-Rad Laboratories, Inc.) and analyzed on a CFX connect Real-Time System (Bio-Rad Laboratories, Inc.). 95˚C for 5 min, followed by 40 cycles of 90˚C for 10 sec and 60˚C for 30 sec, with a final melt-curve analysis. The relative expression level was calculated based on the $2^{-\Delta\Delta Cq}$ method (25).

Western blot analysis. Total proteins were extracted from cells using RIPA buffer (50 mM Tris-HCl pH 7.5, 150 mM NaCl, 0.5% sodium deoxycholate, 1% Triton X-100, 0.1% SDS, 2 mM EDTA) supplemented with protease inhibitor cocktail (Thermo Fisher Scientific, Inc.). Protein concentration was determined using a BCA assay (Thermo Fisher Scientific, Inc.). Equal amounts of protein (20 μg per lane) were resolved by 10% SDS-PAGE, transferred to PVDF membranes (MilliporeSigma) and blocked with 5% skimmed milk at room temperature for 1 h. Membranes were incubated with primary antibodies against MAGEA1 (1:100; cat. no. sc-20033; Santa Cruz Biotechnology, Inc.) and GAPDH (1:4,000; cat. no. sc-32233; Santa Cruz Biotechnology, Inc.), followed by HRP-conjugated secondary antibody (1:5,000; cat. no. 1706516; Bio-Rad Laboratories, Inc.). Bands were visualized using an enhanced chemiluminescence system (Intron Biotechnology, Inc.). Densitometric analysis was performed using ImageJ software, version 1.53k (National Institutes of Health).

Lentiviral transduction for stable knockdown cell construction. Lentiviral transduction was performed using MAGEA1 short hairpin RNAs (shRNAs) lentiviral plasmids (#1 and #2, cat. no. 4100; OriGene Technologies, Inc.) in pGFP-C-shLenti vector. The non-targeting scrambled shRNA, expressing GFP was purchased from OriGene Technologies, Inc.; cat. no. TR30021V). The shRNA sequences used were as follows: shMAGEA1 #1: 5'-TGGAGTCCTTGTTCCGAGCAG TAATCACT-3', shMAGEA1 #2: 5'-CAGTCACAAAGGCAG AAATGCTGGAGAGT-3'. 293T cells (OriGene Technologies, Inc.) were transfected with 5 μg of shRNA plasmids and 3rd-generation lentiviral components (REV, RRE and MD2.G vector) at a weight ratio of 4:2:1:1 using transfection reagents (Promega Corporation). Additional information is provided in Table SI. Media was replaced with antibiotic-free DMEM/10% FBS overnight post-transfection at 37˚C. Viral supernatant was harvested 72 h later and centrifuged at 500 x g at 4˚C for 5 min. HeLa cells were infected with the viral supernatant at a multiplicity of infection (MOI) of 10 for 24 h and selected with 1 μg/ml puromycin for four days after 72 h post-infection (26). Subsequent experiments were conducted 48 h after the selection process. Following initial selection, cells were maintained in 0.8 μg/ml puromycin to preserve stable integration.

Cell proliferation assay. HeLa cells were seeded into 6-well plate at a density of $1.5x10^5$ cells/well for 48 h and $1x10^5$ cells/well 37˚C for 72 h. Each sample was set in triplicate. Cells were detached with EDTA-trypsin and the collected cells were counted with hemocytometer C-Chip (Incyto) using

a light microscope (CKX3-SLP; Olympus Corporation) at x40 magnification.

Wound scratch assay. HeLa cells were cultured in 6 cm plates until they formed a confluent layer. The scratch was inflicted with a sterile 10 μl pipette tip across the center and side of cell monolayer. The medium was removed and washed PBS. Then, 5 ml DMEM without FBS (serum-free) per plate was replaced and incubated as previously described (27). Each image were acquired with light microscope (Ts2R-FL; Nikon Corporation) with a camera for 24, 48, 72 and 96 h following scratch. To determine the wound closure rate, phase contrast images were estimated through the image processing program ImageJ, software, version 1.53k (National Institutes of Health).

Transwell migration and invasion assays. Transwell migration and invasion assays were performed using Transwell plates (SPLInsert hanging; SPL Life Sciences Co., Ltd.). For migration assays, upper chambers with 8 μm pores were coated with 0.2% gelatin. Cells ($5x10^4$ cells/well) were seeded in serum-free DMEM in the upper chamber, with 10% FBS-containing medium in the lower chamber. After 6 h, migrated cells were fixed with methanol at room temperature for 15 min and stained with 1% crystal violet. For invasion assays, upper chambers were coated with 0.2% gelatin and Basement Membrane Extract (BME; equivalent to Matrigel). The pre-coating was performed at 37˚C for 1 h to allow the BME to solidify. Cells ($5x10^4$ cells/well) were seeded similarly and incubated for 24 h. Invaded cells were fixed, stained, and counted in five fields per well.

Cell viability assay. Cell viability was measured by estimating the reduction of 3-(4,5-dimethylthiazol-2) 2,5-diphenyltetrazolium bromide (MTT) to formazan by mitochondrial dehydrogenase. $5x10^3$ cells/well were seeded on 96 well plates a diluted MTT/PBS solution (5 mg/ml) with media was then added to the wells and incubated at 37˚C for 2 h. Living cells reduced MTT to formazan which was quantified by evaluating absorbance at 570 nm wavelength using a microplate reader (GloMax Explorer; Promega Corporation). The cell viability was calculated as CV(%)=(Absorbance of test sample/Absorbance of control) x100.

Cell cycle analysis. For flow cytometric analysis of cell cycle, cells were harvested and fixed with cold 70% ethanol for 48 h at -20˚C. The cells were washed and resuspended in PBS. RNase A (50 μl; 100 μg/ml; Thermo Fisher Scientific, Inc.) was added and incubated at 37˚C water bath for 20 min. Then, the cells were treated with 5 μl propidium iodide (10 mg/ml, Invitrogen; Thermo Fisher Scientific, Inc.) seeded in 96 well plates with density at $1x10^6$ cells/well and incubated at 4˚C in dark until flow cytometry readings. Cell cycle distribution was measured by flow cytometry (CytoFLEX V0-B3-R2 Flow Cytometer; Beckman Coulter, Inc.). The data was analyzed using the CytoFLEX platform (v2.4, Beckman Coulter, Inc.).

Construction of biomimetic 3D culture systems; gelatin methacryloyl (GelMA) colony formation. Lyophilized GelMA was dissolved to 5% GelMA in cell culture media (DMEM) with 0.1% Lithium phenyl-2,4,6-trimethylbenzoylphosphinate. Dissolved GelMA hydrogels were fabricated by dispensing the hydrogel precursors into 24-well culture plate and exposing GelMA with cells at a density of $1.5x10^4$ cells/well to 405 nm UV light for 30 sec. Then, 1 ml of DMEM was added and incubated at 37˚C for seven days. The culture media were replaced every three days to maintain optimal cell growth conditions. Following incubation, the cells were stained with DAPI (MilliporeSigma) at room temperature for 10 min. Each image was captured with a light microscope (Ts2R-FL; Nikon Corporation) with an attached camera.

RNA sequencing (RNA-seq). Cellular RNA was isolated from shNC and shMAGEA1 #1 and #2 using TRIzol® reagent (Invitrogen; Thermo Fisher Scientific, Inc.) according to manufacturer's instructions. TruSeq Stranded mRNA Library Prep Kit (Illumina, Inc.) was used to isolate poly(A)+ mRNA and synthesize cDNA for sequencing library construction. The prepared libraries were sequenced in triplicate on the Illumina NovaSeq 6000 platform (Illumina, Inc.) with a paired-end 150 bp configuration.

Raw sequencing reads were preprocessed using Trimmomatic v0.39 (28), where low-quality bases (Q-score <20) and adapter sequences were removed. The trimmed reads were aligned to the *Homo sapiens* GRCh38 reference genome available on ENSEMBL (release 110; http://ftp.ensembl.org/pub/release-110/fasta/homo_sapiens/dna/) using STAR aligner v2.7.11b (29), and the alignment results were converted to BAM format and sorted using samtools v1.7 (30). The read counts were obtained using FeatureCounts v2.0.8 (31). Normalization of raw count data was conducted using edgeR v4.2.1 (https://bioconductor.org/packages/edgeR/based on the TMM method, followed by GLM fitting and likelihood ratio test for differential expression analysis (32).

Principal Component Analysis (PCA) was performed using the plotPCA function in R to visualize the variance and separation between the control and MAGEA1 knockdown groups based on the normalized gene expression data. Gene expression patterns and enrichment analyses were conducted across three groups (one control and two experimental groups) using the pooled count data to assess gene expression patterns. To visualize this result, a volcano plot was generated using ggrepel v0.9.6 (33) and ggplot2 v3.5.1 (34), where differentially expressed genes (DEGs) were identified based on P-value <0.05. Additionally, the top 10 most statistically significant genes were labeled for emphasis. Gene set enrichment analysis (GSEA) was performed using GSEA software v4.3.3 (35,36) with the MSigDB Hallmark gene sets (h.all.v2024.1.Hs.symbols.gmt) database (37). Heatmaps were created using pheatmap v1.0.12 (38) and RColorBrewer v1.1.3 (39) to compare the expression patterns of enriched gene sets.

Functional annotation of DEGs was conducted using the DAVID web server (40,41), where gene ontology pathway analysis was performed (42,43). DEGs were selected based on overlapping genes between two experimental groups compared with the control [false discovery rate (FDR) <0.01] and classified as upregulated or downregulated according to absolute log2 fold change >0. Furthermore, functional interactions among DEGs were explored using ClueGO v2.5.8 (44,45), with pathway network visualization filtered at term P<0.05.

Tumor xenograft model in nude mice. All animal experimental procedures were performed and approved by accordance with the Catholic University of Korea (approval no. CUK-IACUC-2022-009). Female nude mice (nu/nu; 4-week-old; initial weight, 18-22 g; n=15) were purchased from Orient bio (https://www.orient.co.kr/). The mice were housed in a specific pathogen-free (SPF) facility maintained at 22±2˚C with 55±5% humidity and a 12-h light/dark cycle. To induce tumor genesis, right flank of nude mice (n=5 per group) were subcutaneously inoculated with $1x10^7$ cells transfected with scrambled and shMAGEA1 #1 and #2 resuspended in 150 μl PBS. The mice were randomized after one week and observed for 28 days. Tumor volumes and body weights were calculated twice per week after injection; Tumor volume (mm^3)=length (mm) x width^2 (mm^2) x 1/2. All treated mice were observed and weighed until they met one of the criterion for sacrifice as specified in the IACUC-approved protocol, including tumor volume and body weight thresholds, or until the experimental endpoint was reached. Mice were sacrificed using a gradual-fill CO_2 method at a displacement rate of 30-70% of the chamber volume per min.

Immunohistochemistry (IHC) staining. The tumor tissue samples were fixed with 4% paraformaldehyde at 4˚C for 24 h. Following fixation, the tumor tissues were dehydrated through a graded series of ethanol (70, 80, 90, 95, and 100%), cleared in xylene, and then embedded in paraffin wax at 60˚C. Sections (4 μm thick) were deparaffinized, rehydrated, and permeabilized with 0.1% Triton X-100. IHC was conducted with IHC kit (Abcam; cat. no. ab64264) according to the manufacturer's instructions. Briefly, nonspecific background was blocked using the provided Protein Block for 30 min at room temperature. The sections were incubated with primary antibodies including Ki-67 (1:500; cat. no. HGS-S239; Acro Biosystems Ltd.) and MAGEA1 (1:100; cat. no. sc-20033; Santa Cruz Biotechnology, Inc.) at 4˚C overnight. Then, the sections were incubated with the kit's HRP-conjugated secondary antibody (1:1,000) for 1 h at room temperature. Signal was visualized using DAB solution for 5 min at room temperature, followed by counterstaining with Mayer's Hematoxylin for 2 min at room temperature. Each image was captured with microscope slide scanner (Aperio CS2; Leica Biosystems).

Statistical analysis. All experimental data were performed in triplicate. Statistical significance was determined using GraphPad Prism (v9; Dotmatics) with one-way ANOVA for normally distributed datasets, followed by a suitable post hoc multiple comparisons test (Tukey's multiple comparisons test) to compare the control and MAGEA1 knockdown groups. Error bars in replicate datasets are presented as the standard error of the mean (SEM). $P<0.05$ was considered to indicate a statistically significant difference.

Results

Effects of MAGEA1 on cervical cancer cell proliferation and motility. The association between MAGEA1 expression levels and overall survival across various cancer types was evaluated using Kaplan-Meier survival analysis. This analysis demonstrated that lower MAGEA1 expression in patients with cancer, particularly those with ovarian, lung, gastric, colon, and cervical squamous cell cancers, is markedly associated with improved overall survival, suggesting that high MAGEA1 expression may negatively affect patient prognosis (Fig. S1A-E). Subsequently, the present study analyzed MAGEA1 protein expression levels in various cancer cell lines. Western blot analysis revealed that MAGEA1 expression was markedly elevated in cervical cancer cells (Fig. 1A). To investigate the role of MAGEA1 in cervical cancer, stable MAGEA1 knockdown cell lines (Hela and SiHa) were established by infecting cells with lentiviruses carrying green fluorescence protein (GFP)-tagged constructs encoding either a scrambled shRNA or MAGEA1-specific shRNAs designed to effectively silence MAGEA1 expression. In addition, GFP fluorescence was consistently observed in all groups treated with scrambled shRNA, shMAGEA1 #1 and shMAGEA1 #2, indicating successful and stable transduction using GFP-tagged vectors (Fig. S1F). The cells transduced with shMAGEA1 #1 and shMAGEA1 #2 effectively suppressed both MAGEA1 mRNA and protein expression levels (Figs. 1B and C and S2A and B).

Next, to elucidate the functional role of MAGEA1 in cervical cancer, a series of *in vitro* assays was performed using stable MAGEA1-knockdown cells. The MTT assay revealed that MAGEA1 knockdown markedly reduced cell viability to 77 and 69% compared with the control group (Fig. 1D). Cell proliferation assays also showed that MAGEA1 knockdown markedly reduced cell proliferation at both 48 and 72 h (Figs. 1E and S2C). In wound healing assays performed to assess cellular migration, MAGEA1 depletion inhibited the migratory ability of cervical cancer cells (Fig. 1F and G). In addition, Transwell chamber assays revealed a significant reduction in both the migratory and invasive abilities of MAGEA1-knockdown cells (Figs. 1H, I and S2D), suggesting that MAGEA1 contributes not only to the proliferative capacity of cervical cancer cells but also to their motility.

Effects of MAGEA1 on anchorage-independent cell growth and drug sensitivity. While 2D cell culture systems are widely used in cancer research, they have limitations in accurately replicating the complex 3D architecture and cell-cell interactions of the TME. 3D cell culture using hydrogels is commonly employed for an improved modeling of the native extracellular matrix and intercellular communication. In the field of tissue engineering, hydrogels are regarded as promising scaffolds due to their biocompatibility, tunable mechanical properties, and ability to encapsulate cells and bioactive molecules (46). GelMA hydrogel, a bioink commonly used for 3D bioprinting, is a synthetically modified form of gelatin, in which methacrylate-based groups are introduced into the gelatin side chains through substitution reactions targeting amino (-NH2) and hydroxyl (-OH) groups. The incorporation of methacrylamide groups enhances GelMA's functionality by enabling photo-initiated cross-linking, which facilitates the formation of hydrogels with tunable stiffness and density. These adjustable properties make GelMA an ideal material for constructing biomimetic 3D culture systems. Using GelMA-based hydrogels, the present study established a 3D culture system to evaluate the colony-forming ability of cervical cancer cells under more physiologically relevant conditions (Fig. 2A). In

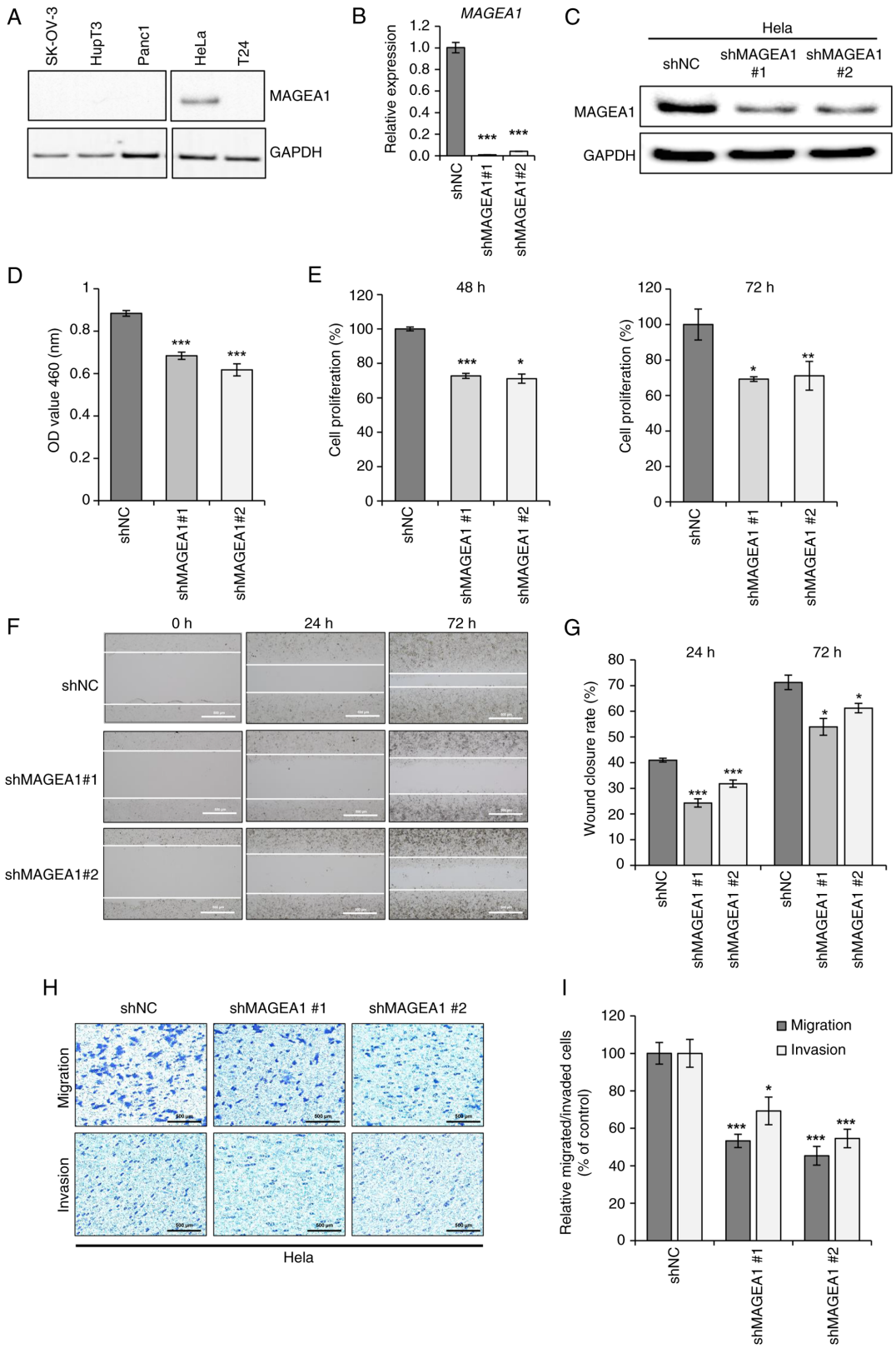

Figure 1. Effects of MAGEA1 knockdown on mRNA/protein expression and cellular functions including proliferation, viability, migration, and invasion. (A) Western blotting detected MAGEA1 expression in SK-OV-3 (ovarian cancer), Panc1 (pancreatic cancer), HupT3 (pancreatic cancer), HeLa (cervical cancer), and T24 (urinary bladder carcinoma). GAPDH was used as a loading control. HeLa was transfected with shMAGEA1 #1 and #2 and shNC was established as a control. (B) Reverse transcription-quantitative PCR and (C) western blot analysis were used to estimate the efficiency of knockdown. (D) Cell viability was determined by MTT assay after 24 h of cell seeding. (E) A significant decrease in cell proliferation was observed in MAGEA1 knockdown compared with control. The number of proliferated cells is presented as a percentage of the control. (F) Representative images from wound scratch at different time points (magnification, x40). (G) Percentages of wound closure at 24 and 72 h are shown as a bar graph. The scratched area and lines were quantified by ImageJ software with the MRI tool. (H) Cell migration and invasion were confirmed by Transwell migration and invasion assays. Representative images of cells are illustrated below. Scale bar, 500 μm. (I) Quantification of migrated and invaded cells in distinct groups. The number of migrated and invaded cells is presented as a percentage of the control. Error bars represent the mean ± SEM. *P<0.05, **P<0.01, ***P<0.005. MAGEA1, MAGE family member A1; sh, short hairpin; NC, negative control.

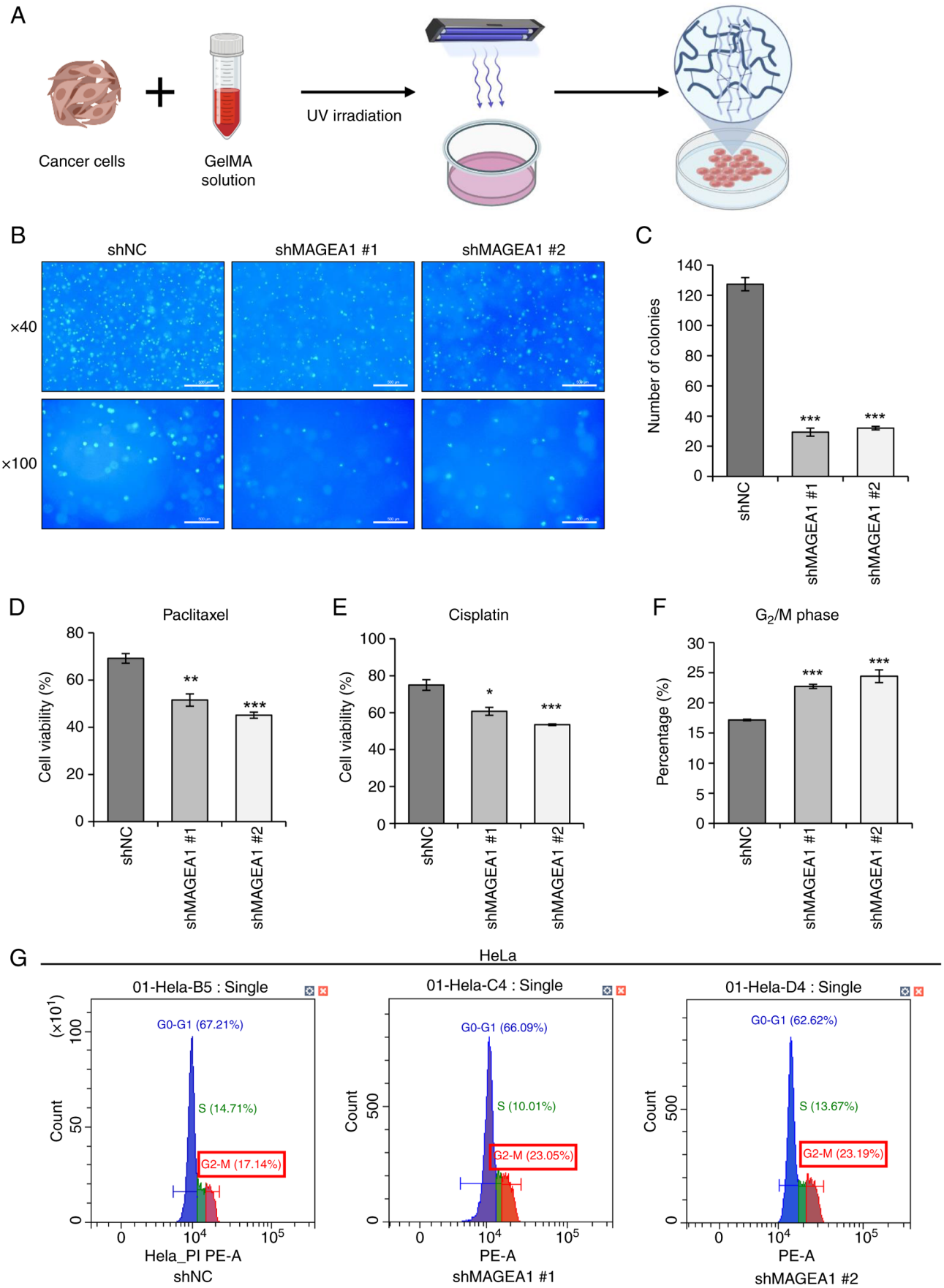

Figure 2. Effect of MAGEA1 knockdown on colony formation, chemosensitivity, and cell cycle progression. (A) A Schematic diagram of 3D experimental design. (B) Fluorescent microscope images of DAPI staining (magnification x40, x100). Scale bar, 500 μm. (C) Quantification of colony formation with 8 or more colonies on GelMA. Cells were treated with (D) 1 μM of paclitaxel and (E) 20 μM of cisplatin for 48 h and cell viability was measured by MTT assays. (F) Cells were stained with PI and analyzed using Cytexpert software (v2.4). (G) Representative DNA content histograms showing distributions across G0-G1, S, and G_2-M phases in each group samples. Error bars represent the mean ± SEM. *P<0.05, **P<0.01, ***P<0.005. MAGEA1, MAGE family member A1; GelMA, gelatin methacryloyl.

the colony formation assay, most cells in the control group formed colonies consisting of 6-8 cells, whereas the MAGEA1 knockdown groups predominantly formed smaller colonies composed of 2-4 cells (Fig. 2B). Notably, the number of colonies containing eight or more cells was notably reduced in the MAGEA1 knockdown groups, accounting for only 29 and 32% relative to the control group (Fig. 2C), suggesting that MAGEA1 is closely associated with anchorage-independent cell growth in 3D environments.

Paclitaxel is a widely used chemotherapeutic diterpenoid alkaloid that exerts its anti-cancer effects by promoting tubulin polymerization and inhibiting mitosis (47). Cisplatin, a platinum-based chemotherapeutic agent, acts as a DNA-damaging compound that inhibits tumor growth. Through preliminary dose-response experiments, we determined the concentrations of paclitaxel (1 μM) and cisplatin (20 μM) that inhibit ~30% of cell growth in HeLa cells. Treatment with these concentrations of paclitaxel and cisplatin resulted in a significant increase in drug sensitivity in MAGEA1 knockdown cells compared with the control group (Fig. 2D and E), suggesting that MAGEA1 may be involved in drug resistance in cervical cancer cells.

Based on the observation that MAGEA1 is closely associated with cancer cell growth, the present study analyzed the cell cycle distribution of cervical cancer cells using flow cytometry. As a result, the proportion of cells in the G_2/M phase was markedly increased in the MAGEA1 knockdown group compared with the control group (Fig. 2F and G). This accumulation of cells in the G_2/M phase suggested that MAGEA1 depletion impaired the ability of cervical cancer cells to progress through mitosis, potentially contributing to the reduced proliferation observed in knockdown cells.

MAGEA1 alters the expression of genes related to the cell cycle, hypoxia, and apoptosis. To investigate MAGEA1-mediated regulation of gene expression, RNA-seq was performed on both MAGEA1 knockdown cells and control cells. Principal component analysis revealed a clear separation between control and MAGEA1 knockdown groups, indicating distinct transcriptomic differences (Fig. S3A). A total of 2,289 upregulated and 2,016 downregulated DEGs were identified between the control and MAGEA1 knockdown groups (FDR <0.01; |log2 fold change|>0). A heatmap illustrated the clustering and expression patterns of these DEGs between shNC- and shMAGEA1-transfected cells, offering a comprehensive overview of transcriptomic alterations (Fig. 3A). In addition, a volcano plot depicted the distribution of fold changes, highlighting the most markedly dysregulated genes (Fig. S3B). ClueGO-based Gene Ontology Biological Process analysis revealed significant upregulation of pathways related to apoptotic processes, cell cycle regulation and DNA damage response, while pathways associated with metabolic functions, including ATP synthesis, nucleotide biosynthesis, oxidative phosphorylation, and lipid metabolism, were substantially downregulated (Fig. 3B). Functional enrichment network analysis revealed crosstalk among upregulated pathways, with apoptotic processes, DNA damage response, and cell cycle regulation forming interconnected clusters (Fig. 3C). Conversely, the downregulated gene network was predominantly enriched in metabolic pathways, including oxidative phosphorylation, the electron transport chain, and phospholipid metabolism (Fig. S3C).

GSEA and expression heatmaps confirmed significant positive enrichment of apoptosis and G_2/M checkpoint gene sets in MAGEA1 knockdown cells, whereas hypoxia-related pathways exhibited negative enrichment (Fig. 4A-D). To validate the RNA-sequencing results, several key DEGs were selected for confirmation via RT-qPCR. The data showed elevated mRNA expression levels of *POU2AF2* and *Pax5* (Fig. 4E; Tables SII and SIII). POU2AF2, a regulator of tuft cell differentiation, may be inversely associated with the increased risk of cancer development (48). Pax5 is primarily known as a B cell-specific transcription factor and also exhibits tumor-suppressive activity by inducing cell cycle arrest in primary effusion lymphoma (49). In addition, RT-qPCR analysis confirmed the downregulation of *BIRC3*, and *CDC45* (Fig. 4F; Tables SII and SIII). These genes are associated with cervical cancer cell survival and the inhibition of apoptosis (50). In particular, CDC45, a gene implicated in cervical cancer progression, may contribute to G_2/M phase cell cycle arrest and suppressed cell proliferation (51). POU2AF2, Pax5, BIRC3 and CDC45 were prioritized because they exhibit biological relevance to MAGEA1-associated pathways, as previous evidence indicates functional interactions or co-regulation with MAGEA1 in tumor progression.

Collectively, these transcriptomic analyses demonstrated that MAGEA1 knockdown induced profound alterations in the gene expression profile of cervical cancer cells, particularly impacting pathways related to cell survival, DNA damage response and cellular metabolism. These molecular changes identify MAGEA1 as a key regulator of cervical cancer progression and emphasize its potential as a promising therapeutic target.

MAGEA1 depletion suppresses in vivo tumor growth. To evaluate the effect of MAGEA1 on *in vivo* tumor growth, HeLa cells stably expressing shNC, shMAGEA1 #1, or shMAGEA1 #2 were subcutaneously injected into BALB/c nude mice. Tumor size and mouse body weight were measured twice weekly, and at the end of the experiment, tumors were excised for imaging and weighed (Fig. 5A). Monitoring of mouse body weights throughout the experiment revealed no significant differences between the control group and the shMAGEA1 groups (Fig. S4A). During the three-week observation period, tumors in the control group grew progressively, while those in the shMAGEA1 #1 and #2 groups showed markedly slower growth rates. On day 25, analysis of individual tumor volumes showed that the mean tumor volumes in the shMAGEA1 #1 group (413.97±45.35 mm^3) and shMAGEA1 #2 group (430.24±122.87 mm^3) were reduced by 49.3 and 48.3%, respectively, compared with the control group (816.84±156.23 mm^3; Fig. 5B). Tumor weight measurements demonstrated that tumors in the shMAGEA1 #1 group (0.34 g) and shMAGEA1 #2 group (0.35 g) were markedly reduced compared with the control group (0.67 g; Fig. 5C and D). IHC analysis of tumor tissues confirmed the sustained suppression of MAGEA1 protein expression in MAGEA1 knockdown tumors (Fig. 5E, top). Furthermore, immunostaining for the proliferation marker Ki-67 showed that the number of

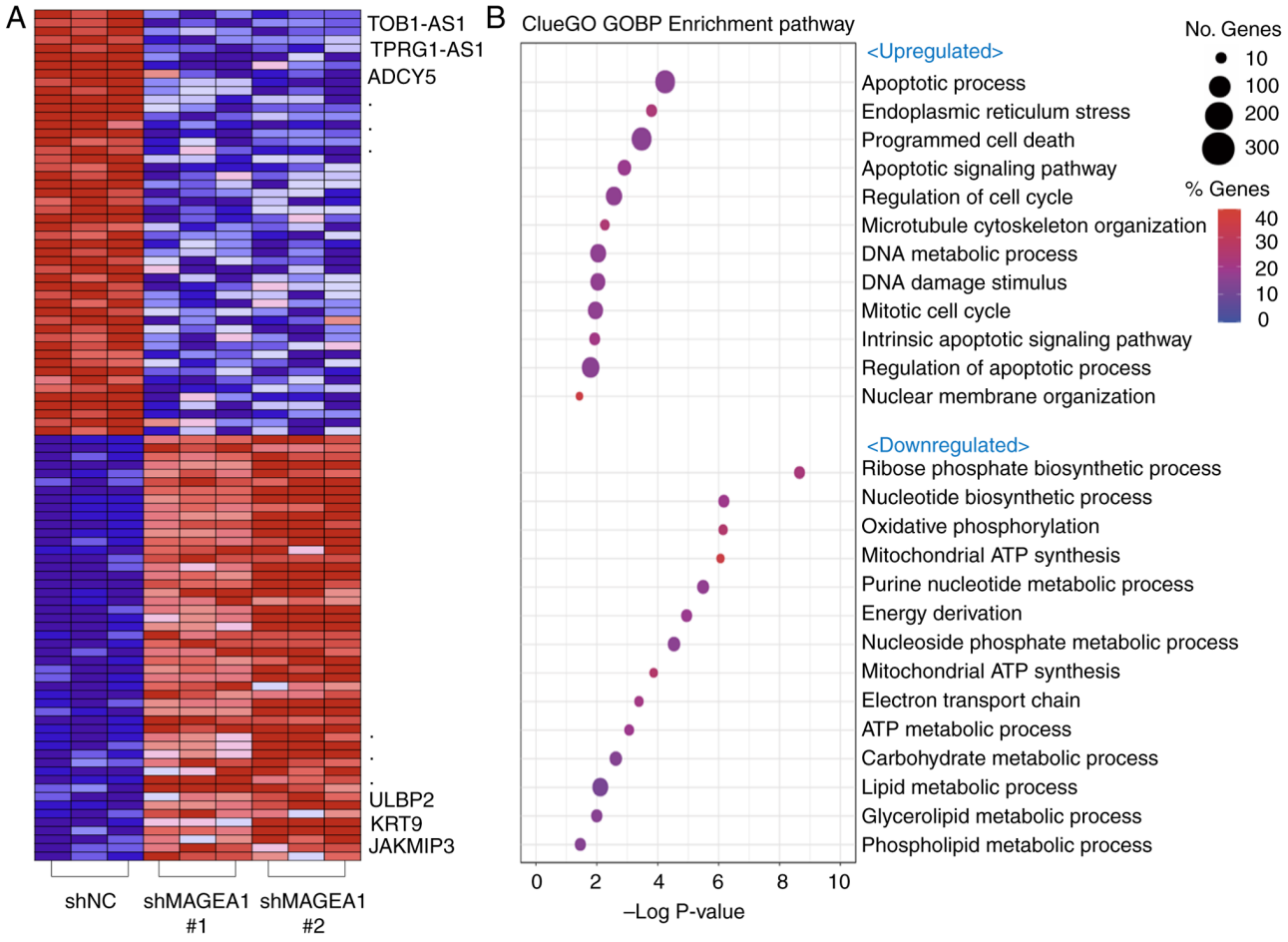

Figure 3. Comprehensive transcriptomic and functional analysis of MAGEA1 knockdown in HeLa cells. (A) Heatmap representing DEGs between shNC and shMAGEA1-transfected HeLa cells based on RNA sequencing data. (B) ClueGO pathway network analysis showing markedly altered biological processes following MAGEA1 knockdown. (C) Functional enrichment network of upregulated genes (Hela_FDR001_logFC0_UP_GOBP) following MAGEA1 knockdown in HeLa cells. MAGEA1, MAGE family member A1; DEGs, differentially expressed genes; sh, short hairpin; NC, negative control.

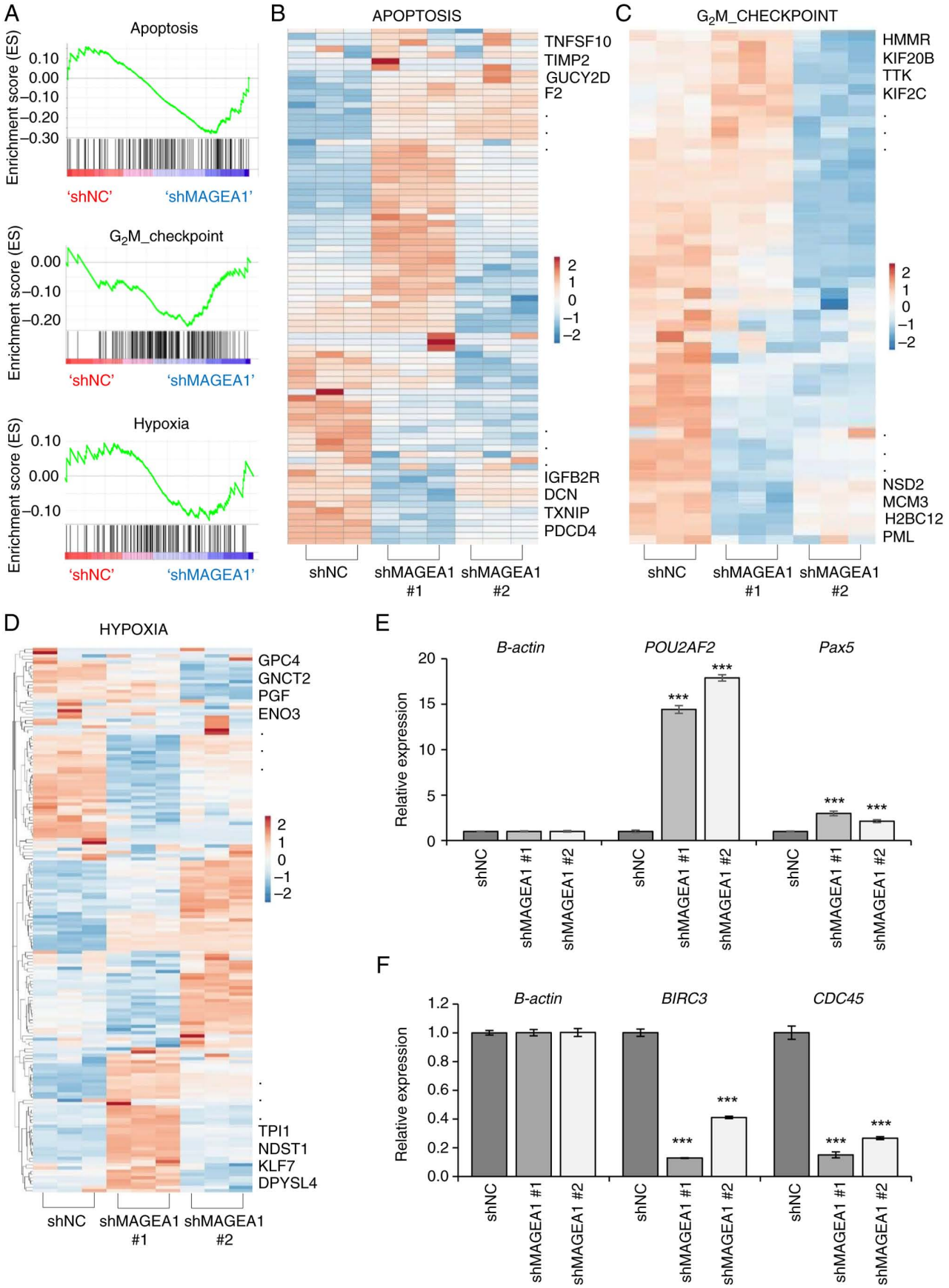

Figure 4. Gene expression changes and validation of key DEGs following MAGEA1 knockdown. (A) GSEA plots showing significant enrichment of genes. Pathways markedly enriched in the shMAGEA1 group including apoptosis, G_2M checkpoint, and DNA repair, indicating enhanced cell death signaling and disrupted cell cycle regulation. (B-D) Heatmap shows expression levels of genes in G_2/M checkpoint, apoptosis and hypoxia pathways following MAGEA1 knockdown vs. control (shNC) cells. Red indicates upregulated genes; blue indicates downregulated genes. (E and F) Quantitative PCR of selected differentially expressed genes. Error bars represent the mean ± SEM. ***P<0.005. DEGs, differentially expressed genes; MAGEA1, MAGE family member A1; GSEA, gene set enrichment analysis; sh, short hairpin; NC, negative control.

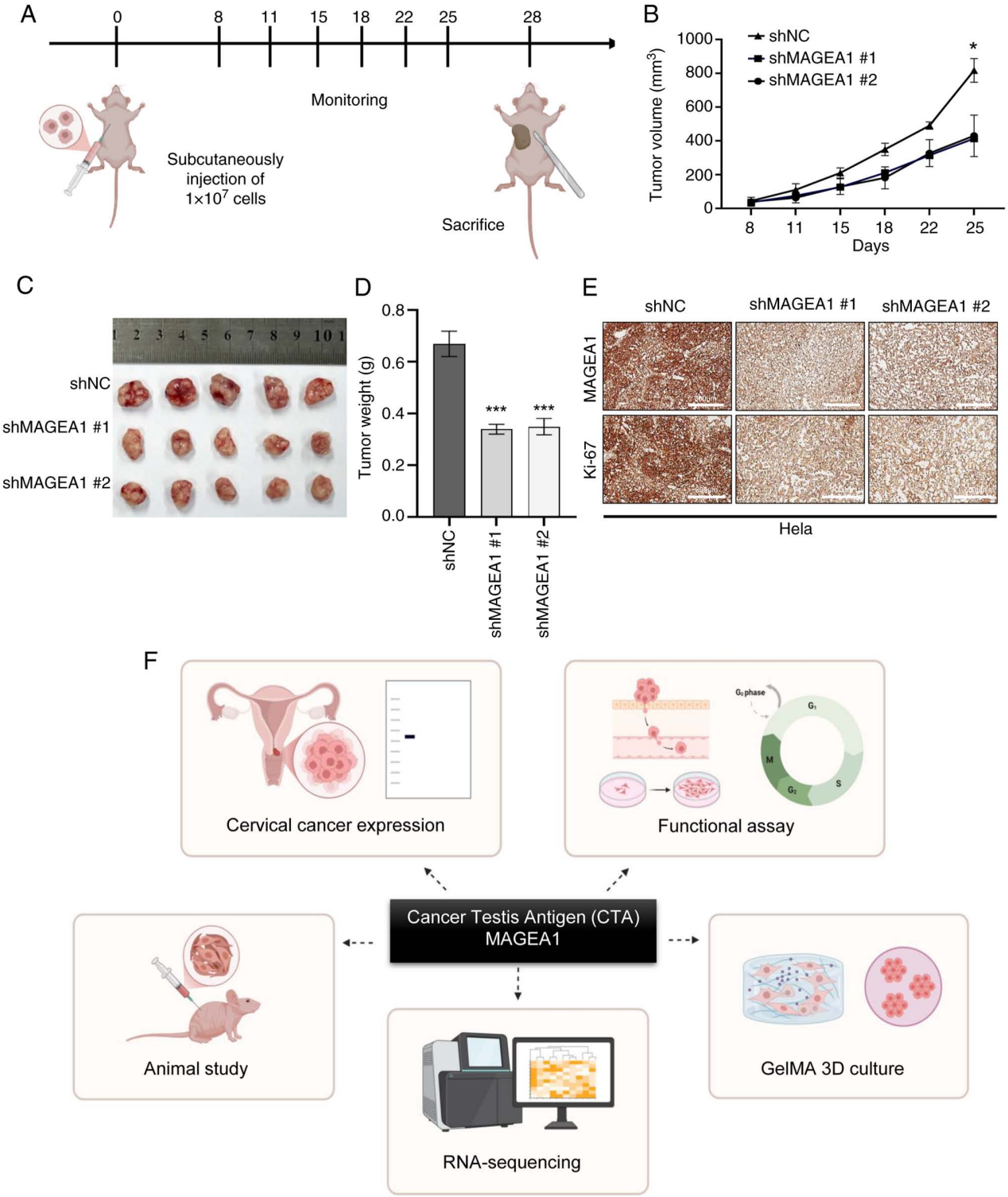

Figure 5. MAGEA1 knockdown suppresses tumorigenicity of cervical cancer cells *in vivo*. (A) Schematic diagram of the xenograft experiment using BALB/c nude mice injected with HeLa cells transfected with shNC, shMAGEA1 #1, or shMAGEA1 #2. (B) Representative images of excised tumors from each group at day 28 post-injection. (C) Tumor growth curves showing tumor volumes measured twice a week. Mice injected with shMAGEA1 HeLa cells exhibited markedly reduced tumor volumes compared with the control group. (D) Final tumor weights measured at the end of the experiment (day 30). (E) Representative immunohistochemical staining images showing MAGEA1 and Ki-67 expression in tumor tissues from mice injected with HeLa cells transfected with shNC, shMAGEA1 #1, or shMAGEA1 #2. Scale bar, 300 μm. (F) Comprehensive study of MAGEA1 function and expression in cervical cancer. Error bars represent the mean ± SEM. *P<0.05, ***P<0.005. MAGEA1, MAGE family member A1; sh, short hairpin; NC, negative control.

Ki-67-positive cells was markedly reduced in shMAGEA1 tumors (Fig. 5E, bottom). Collectively, these results clearly demonstrated that MAGEA1 depletion effectively suppresses *in vivo* tumor growth in cervical cancer.

Discussion

The present study revealed through a series of functional assays that MAGEA1 was highly upregulated in cervical

cancer and functioned as a key regulator of tumor progression (Fig. 5F). Knockdown of MAGEA1 markedly inhibited cell proliferation, migration, invasion and tumor growth, while enhancing chemosensitivity. The present study further explained the molecular mechanisms underlying the role of MAGEA1 in cervical cancer through comprehensive RNA-seq analysis. The bioinformatics evaluation disclosed significant alterations in key cellular pathways following MAGEA1 knockdown, notably the upregulation of apoptosis, DNA repair and cell cycle checkpoint pathways. Additionally, the downregulation of metabolic pathways, including ATP metabolism and lipid metabolism, suggested that MAGEA1 plays a critical role in regulating cancer cell metabolism, a hallmark of cancer progression. To validate the *in vitro* findings in a more physiologically relevant context, a xenograft model was established using BALB/c nude mice. Especially, both shMAGEA1 groups exhibited markedly reduced tumor growth and volume compared with the control group, strongly supporting the *in vivo* tumor-suppressive effect of MAGEA1 knockdown. These *in vivo* findings were consistent with the *in vitro* data and further validated MAGEA1 as a key regulator of cervical cancer progression.

MAGEA1 is a member of the CTA family and is normally restricted to immune-privileged tissues such as the testis. However, it is aberrantly re-expressed in a wide range of malignancies, including melanoma, lung, gastric, colorectal and breast cancers, as well as hematologic cancers (22,52-56). High MAGEA1 expression has been associated with aggressive clinicopathological features and poor patient survival, particularly in breast, lung and gastric cancer (57). In gastric and colorectal cancers, MAGEA1 genes have been implicated in carcinogenesis and proposed as diagnostic markers of malignant transformation (53,58). Functional studies in lung adenocarcinoma further indicate that MAGEA1 promotes tumor growth and may represent a promising target for antigen-specific immunotherapy (59). However, compared with other CTAs, MAGEA1 remains relatively poorly understood. Notably, to the best of the authors' knowledge, no previous studies have established a relationship between MAGEA1 and cervical cancer. In the present study, the RNA-seq analysis provided the first evidence that MAGEA1 may serve as a novel biomarker not only for cervical cancer but also potentially for a broad spectrum of types of cancer. To evaluate the potential of MAGEA1 as a therapeutic target in cervical cancer, the present study investigated the effects of shRNA-mediated MAGEA1 knockdown on cell proliferation, migration, invasion and colony formation. Consistent upregulation of MAGEA1 was observed in cervical cancer cells and the present study demonstrated that MAGEA1 played a key role in promoting cell migration, invasion, wound healing and anchorage-independent growth, consistent with previous findings in melanoma and breast cancer.

Notably, MAGEA1 knockdown markedly increased sensitivity to chemotherapeutic agents, suggesting a potential involvement in drug resistance mechanisms, implying that targeting MAGEA1 could enhance the therapeutic efficacy of conventional chemotherapies in cervical cancer treatment. Despite favorable 5-year survival rates >80% for early-stage cervical cancer, clinical data indicates that in young women under 30 years, high-risk HPV infections can rapidly progress to high-grade lesions within two years (60). Therefore, the identification and functional characterization of host proteins interacting with HPV oncoproteins remains a significant challenge in advancing cervical cancer therapy. Understanding these interactions could provide critical insights into cervical tumorgenesis and contribute to the development of novel therapeutic strategies targeting these magnalities.

Nevertheless, translating these findings into clinical applications will require further investigation to optimize the delivery of MAGEA1-targeted agents and assess potential off-target effects in complex physiological environments. Future research should focus on clarifying the molecular interactions between MAGEA1 and HPV oncoproteins, evaluating synergistic effects with conventional therapies, and investigating the role of MAGEA1 in immune evasion mechanisms. Such studies could provide the basis for personalized immunotherapeutic strategies, utilizing the immunogenic properties of MAGEA1 as a cancer-testis antigen.

Acknowledgements

The schematics of Figs. 2 and 5 were created by the authors using images provided by BioRender (https://biorender.com/).

Funding

The present study was funded by the Brain Korea 21, grant no. M2022B002600003, Korea Health Industry Development Institute, grant no. RS-2025-02214206 and the Ministry of Food and Drug Safety in Korea, grant nos. 22213MFDS421 and RS-2025-02213409.

Availability of data and materials

The data generated in the present study may be requested from the corresponding author. All RNA-seq data generated in this may be found in the NCBI BioProject database (https://www.ncbi.nlm.nih.gov/bioproject) under accession number PRJNA1362940 or at the following URL: https://www.ncbi.nlm.nih.gov/bioproject/PRJNA1362940.

Authors' contributions

Conceptualization was by AK, JK, WK, JWY and HY. AK, JK, WK, KM, SC, MJ, JL, JWY and HY wrote the original draft. WK, JWY and HY were responsible for writing, reviewing and editing. JWY and HY confirm the authenticity of all the raw data. All authors read and approved the final manuscript.

Ethics approval and consent to participate

Not applicable.

Patient consent for publication

Not applicable.

Competing interests

The authors declare they have no competing interests.

References

1. Causin RL, Freitas AJA, Hidalgo Filho CMT, Reis RD, Reis RM and Marques MMC: A systematic review of MicroRNAs involved in cervical cancer progression. Cells 10: 668, 2021.
2. Plante M, Kwon JS, Ferguson S, Samouëlian V, Ferron G, Maulard A, de Kroon C, Van Driel W, Tidy J, Williamson K, *et al*: Simple versus radical hysterectomy in women with low-risk cervical cancer. N Engl J Med 390: 819-829, 2024.
3. Wang M, Huang K, Wong MCS, Huang J, Jin Y and Zheng ZJ: Global cervical cancer incidence by histological subtype and implications for screening methods. J Epidemiol Glob Health 14: 94-101, 2024.
4. Cohen CM, Wentzensen N, Castle PE, Schiffman M, Zuna R, Arend RC and Clarke MA: Racial and ethnic disparities in cervical cancer incidence, survival, and mortality by histologic subtype. J Clin Oncol 41: 1059-1068, 2023.
5. Yang ST, Wang PH, Liu HH, Chang CW, Chang WH and Lee WL: Cervical cancer: Part II the landscape of treatment for persistent, recurrent and metastatic diseases (I). Taiwan J Obstet Gynecol 63: 637-650, 2024.
6. Lai W, Liao J, Li X, Liang P, He L, Huang K, Liang X and Wang Y: Characterization of the microenvironment in different immune-metabolism subtypes of cervical cancer with prognostic significance. Front Genet 14: 1067666, 2023.
7. Craig AJ, Garcia-Lezana T, Ruiz de Galarreta M, Villacorta-Martin C, Kozlova EG, Martins-Filho SN, von Felden J, Ahsen ME, Bresnahan E, Hernandez-Meza G, *et al*: Transcriptomic characterization of cancer-testis antigens identifies MAGEA3 as a driver of tumor progression in hepatocellular carcinoma. PLoS Genet 17: e1009589, 2021.
8. Vlasenkova R, Konysheva D, Nurgalieva A and Kiyamova R: Characterization of cancer/testis antigens as prognostic markers of ovarian cancer. Diagnostics (Basel) 13: 3092, 2023.
9. Chen L, Wu Q, Xu X, Yang C, You J, Chen F and Zeng Y: Cancer/testis antigen LDHC promotes proliferation and metastasis by activating the PI3K/Akt/GSK-3β-signaling pathway and the in lung adenocarcinoma. Exp Cell Res 398: 112414, 2021.
10. Danilova A, Misyurin V, Novik A, Girdyuk D, Avdonkina N, Nekhaeva T, Emelyanova N, Pipia N, Misyurin A and Baldueva I: Cancer/testis antigens expression during cultivation of melanoma and soft tissue sarcoma cells. Clin Sarcoma Res 10: 3, 2020.
11. Cui Z, Chen Y, Hu M, Lin Y, Zhang S, Kong L and Chen Y: Diagnostic and prognostic value of the cancer-testis antigen lactate dehydrogenase C4 in breast cancer. Clin Chim Acta 503: 203-209, 2020.
12. Yu QY, Wang ZW, Zhou MY, Li SF and Liao XH: MAGE-A3 regulates tumor stemness in gastric cancer through the PI3K/AKT pathway. Aging (Albany NY) 14: 9579-9598, 2022.
13. Bai R and Yuan C: Kita-kyushu lung cancer antigen-1 (KK-LC-1): A promising cancer testis antigen. Aging Dis 13: 1267-1277, 2022.
14. Wei R, Dean DC, Thanindratarn P, Hornicek FJ, Guo W and Duan Z: Cancer testis antigens in sarcoma: Expression, function and immunotherapeutic application. Cancer Lett 479: 54-60, 2020.
15. Wang Z, Liu Z and Wu S: Long non-coding RNA CTA sensitizes osteosarcoma cells to doxorubicin through inhibition of autophagy. Oncotarget 8: 31465-31477, 2017.
16. Yang P, Meng M and Zhou Q: Oncogenic cancer/testis antigens are a hallmarker of cancer and a sensible target for cancer immunotherapy. Biochim Biophys Acta Rev Cancer 1876: 188558, 2021.
17. Hikmet F, Rassy M, Backman M, Méar L, Mattsson JSM, Djureinovic D, Botling J, Brunnström H, Micke P and Lindskog C: Expression of cancer-testis antigens in the immune microenvironment of non-small cell lung cancer. Mol Oncol 17: 2603-2617, 2023.
18. Ren S, Zhang Z, Li M, Wang D, Guo R, Fang X and Chen F: Cancer testis antigen subfamilies: Attractive targets for therapeutic vaccine (review). Int J Oncol 62: 71, 2023.
19. Weon JL and Potts PR: The MAGE protein family and cancer. Curr Opin Cell Biol 37: 1-8, 2015.
20. Yang SW, Huang X, Lin W, Min J, Miller DJ, Mayasundari A, Rodrigues P, Griffith EC, Gee CT, Li L, *et al*: Structural basis for substrate recognition and chemical inhibition of oncogenic MAGE ubiquitin ligases. Nat Commun 11: 4931, 2020.
21. Laduron S, Deplus R, Zhou S, Kholmanskikh O, Godelaine D, De Smet C, Hayward SD, Fuks F, Boon T and De Plaen E: MAGE-A1 interacts with adaptor SKIP and the deacetylase HDAC1 to repress transcription. Nucleic Acids Res 32: 4340-4350, 2004.
22. Wang D, Wang J, Ding N, Li Y, Yang Y, Fang X and Zhao H: MAGE-A1 promotes melanoma proliferation and migration through C-JUN activation. Biochem Biophys Res Commun 473: 959-965, 2016.
23. Lian Y, Meng L, Ding P and Sang M: Epigenetic regulation of MAGE family in human cancer progression-DNA methylation, histone modification, and non-coding RNAs. Clin Epigenetics 10: 115, 2018.
24. Oh C, Kim HR, Oh S, Ko JY, Kim Y, Kang K, Yang Y, Kim J, Park JH, Roe JS and Yoo KH: Epigenetic upregulation of MAGE-A isoforms promotes breast cancer cell aggressiveness. Cancers (Basel) 13: 3176, 2021.
25. Livak KJ and Schmittgen TD: Analysis of relative gene expression data using real-time quantitative PCR and the 2(-Delta Delta C(T)) method. Methods 25: 402-408, 2001.
26. Matentzoglu K and Scheffner M: Ubiquitin-fusion protein system: A powerful tool for ectopic protein expression in mammalian cells. Biotechniques 46: 21-22, 24, 26, 2009.
27. Tsai HC, Li YC, Hsu SH, Young TH and Chen MH: Inhibition of growth and migration of oral and cervical cancer cells by citrus polyphenol. J Formos Med Assoc 115: 171-185, 2016.
28. Bolger AM, Lohse M and Usadel B: Trimmomatic: A flexible trimmer for Illumina sequence data. Bioinformatics 30: 2114-2120, 2014.
29. Dobin A, Davis CA, Schlesinger F, Drenkow J, Zaleski C, Jha S, Batut P, Chaisson M and Gingeras TR: STAR: Ultrafast universal RNA-seq aligner. Bioinformatics 29: 15-21, 2013.
30. Li H, Handsaker B, Wysoker A, Fennell T, Ruan J, Homer N, Marth G, Abecasis G and Durbin R; 1000 Genome Project Data Processing Subgroup: The sequence alignment/map format and SAMtools. Bioinformatics 25: 2078-2079, 2009.
31. Liao Y, Smyth GK and Shi W: featureCounts: An efficient general purpose program for assigning sequence reads to genomic features. Bioinformatics 30: 923-930, 2014.
32. Chen Y, Chen L, Lun ATL, Baldoni PL and Smyth GK: edgeR v4: Powerful differential analysis of sequencing data with expanded functionality and improved support for small counts and larger datasets. Nucleic Acids Res 53: gkaf018, 2025.
33. Wickham H: Data analysis. In: ggplot2: Elegant graphics for data analysis. Springer, pp189-201, 2016.
34. Wickham H: ggplot2: Elegant graphics for data analysis. 2nd edition, Springer, New York, 2009.
35. Subramanian A, Tamayo P, Mootha VK, Mukherjee S, Ebert BL, Gillette MA, Paulovich A, Pomeroy SL, Golub TR, Lander ES and Mesirov JP: Gene set enrichment analysis: A knowledge-based approach for interpreting genome-wide expression profiles. Proc Natl Acad Sci USA 102: 15545-15550, 2005.
36. Mootha VK, Lindgren CM, Eriksson KF, Subramanian A, Sihag S, Lehar J, Puigserver P, Carlsson E, Ridderstråle M, Laurila E, *et al*: PGC-1alpha-responsive genes involved in oxidative phosphorylation are coordinately downregulated in human diabetes. Nat Genet 34: 267-273, 2003.
37. Liberzon A, Birger C, Thorvaldsdóttir H, Ghandi M, Mesirov JP and Tamayo P: The molecular signatures database (MSigDB) hallmark gene set collection. Cell Syst 1: 417-425, 2015.
38. Kolde R and Kolde MR: Package 'pheatmap'. R Package 1: 790, 2015.
39. Neuwirth E: RColorBrewer: Colorbrewer palettes. R Package Version 1.1-3, 2014.
40. Sherman BT, Hao M, Qiu J, Jiao X, Baseler MW, Lane HC, Imamichi T and Chang W: DAVID: A web server for functional enrichment analysis and functional annotation of gene lists (2021 update). Nucleic Acids Res 50 (W1): W216-W221, 2022.
41. Huang DW, Sherman BT and Lempicki RA: Systematic and integrative analysis of large gene lists using DAVID bioinformatics resources. Nat Protoc 4: 44-57, 2009.
42. Ashburner M, Ball CA, Blake JA, Botstein D, Butler H, Cherry JM, Davis AP, Dolinski K, Dwight SS, Eppig JT, *et al*: Gene ontology: Tool for the unification of biology. The gene ontology consortium. Nat Genet 25: 25-29, 2000.
43. Gene Ontology Consortium; Aleksander SA, Balhoff J, Carbon S, Cherry JM, Drabkin HJ, Ebert D, Feuermann M, Gaudet P, Harris NL, *et al*: The gene ontology knowledgebase in 2023. Genetics 224: iyad031, 2023.
44. Bindea G, Mlecnik B, Hackl H, Charoentong P, Tosolini M, Kirilovsky A, Fridman WH, Pagès F, Trajanoski Z and Galon J: ClueGO: A Cytoscape plug-in to decipher functionally grouped gene ontology and pathway annotation networks. Bioinformatics 25: 1091-1093, 2009.

45. Bindea G, Galon J and Mlecnik B: CluePedia Cytoscape plugin: Pathway insights using integrated experimental and in silico data. Bioinformatics 29: 661-663, 2013.
46. Imere A, Foster NC, Hajiali H, Okur KE, Wright AL, Barroso IA and Haj AJE: Enhanced chondrogenic potential in GelMA-based 3D cartilage model via Wnt3a surface immobilization. Sci Rep 14: 15022, 2024.
47. Qiao JX, Guo DY, Tian H, Wang ZP, Fan QQ, Tian Y, Sun J, Zhang XF, Zou JB, Cheng JX, *et al*: Research progress of paclitaxel nanodrug delivery system in the treatment of triple-negative breast cancer. Mater Today Bio 29: 101358, 2024.
48. Rajasekaran V, Harris BT, Osborn RT, Smillie C, Donnelly K, Bacou M, Esiri-Bloom E, Ooi LY, Allan M, Walker M, *et al*: Genetic variation at 11q23.1 confers colorectal cancer risk by dysregulation of colonic tuft cell transcriptional activator POU2AF2. Gut 74: 787-803, 2025.
49. Goto H, Kariya R, Kudo E, Katano H and Okada S: PAX5 functions as a tumor suppressor by RB-E2F-mediated cell cycle arrest in Kaposi sarcoma-associated herpesvirus-infected primary effusion lymphoma. Neoplasia 56: 101035, 2024.
50. Bloomstein JD, von Eyben R, Chan A, Rankin EB, Fregoso DR, Wang-Chiang J, Lee L, Xie LX, David SM, Stehr H, *et al*: Validated limited gene predictor for cervical cancer lymph node metastases. Oncotarget 11: 2302-2309, 2020.
51. He Z, Wang X, Yang Z, Jiang Y, Li L, Wang X, Song Z, Wang X, Wan J, Jiang S, *et al*: Expression and prognosis of CDC45 in cervical cancer based on the GEO database. PeerJ 9: e12114, 2021.
52. Yi E, Chang JE, Leem C, Jeon CH and Jheon S: Association of MAGE A1-6 expression with lung cancer progression. J Cancer 8: 1324-1329, 2017.
53. Lian Y, Sang M, Gu L, Liu F, Yin D, Liu S, Huang W, Wu Y and Shan B: MAGE-A family is involved in gastric cancer progression and indicates poor prognosis of gastric cancer patients. Pathol Res Pract 213: 943-948, 2017.
54. Almutairi MH, Alotaibi MM, Alonaizan R, Alrefaei AF and Almutairi BO: Identification of MAGE-A family genes in colon cancer patients and their expression mechanism. J King Saud Univ Sci 34: 102251, 2022.
55. Mi Y, Liu F, Liang X, Liu S, Huang X, Sang M and Geng C: Tumor suppressor let-7a inhibits breast cancer cell proliferation, migration and invasion by targeting MAGE-A1. Neoplasma 66: 54-62, 2019.
56. Suyama T, Ohashi H, Nagai H, Hatano S, Asano H, Murate T, Saito H and Kinoshita T: The MAGE-A1 gene expression is not determined solely by methylation status of the promoter region in hematological malignancies. Leuk Res 26: 1113-1118, 2002.
57. Jin S, Cao S, Li J, Meng Q, Wang C, Yao L, Lang Y, Cao J, Shen J, Pan B, *et al*: Cancer/testis antigens (CTAs) expression in resected lung cancer. Onco Targets Ther 11: 4491-4499, 2018.
58. Tarnowski M, Czerewaty M, Deskur A, Safranow K, Marlicz W, Urasińska E, Ratajczak MZ and Starzyńska T: Expression of cancer testis antigens in colorectal cancer: New prognostic and therapeutic implications. Dis Markers 2016: 1987505, 2016.
59. Fanipakdel A, Seilanian Toussi M, Rezazadeh F, Mohamadian Roshan N and Javadinia SA: Overexpression of cancer-testis antigen melanoma-associated antigen A1 in lung cancer: A novel biomarker for prognosis, and a possible target for immunotherapy. J Cell Physiol 234: 12080-12086, 2019.
60. Lei J, Ploner A, Elfström KM, Wang J, Roth A, Fang F, Sundström K, Dillner J and Sparén P: HPV vaccination and the risk of invasive cervical cancer. N Engl J Med 383: 1340-1348, 2020.